International Journal of Applied Engineering Research ISSN 0973-4562 Volume 12, Number 23 (2017) pp. 13843-13846

Assessment of Healthy Human Aortic Arch Hemodynamics using Computational Fluid Dynamics (CFD)

Taewon Seo*, and Do-Il Kim**

**Department of Mechanical and Automotive Engineering, Andong National University, Andong, 36729, South Korea.*
***CEO, Water Pipe CO LTD, Andong, 36656, South Korea.*
**Orcid: 0000-0003-4653-8810*

Abstract

In this study, CT images of human aorta are used to extract and to analyze the blood flow through the human aortic arch geometry. The CFD simulation uses the commercial ANSYS 18.1 based on a finite volume method for solving the Navier-Stokes equations. The simulation is conducted to understand the flow phenomena in the aortic model. Thus, we investigate the hemodynamic factors, such as secondary flow, wall pressure and wall shear stresses (WSS) in the aortic arch model. The axial velocity profiles in the ascending aorta is skewed toward the inner wall of the curvature and the helical flow observed in the ascending aorta. It is noted that there was a region of severely higher WSS at distal sites of branches at the top of aortic arch.

Keywords: Computational Fluid Dynamics (CFD), Aortic Arch, Hemodynamics, Computed Tomography (CT), Wall Shear Stress (WSS)

INTRODUCTION

The aorta is the largest artery in the human body, originating from the left ventricle of the heart and begins as the ascending aorta, turns into the aortic arch and takes the descending thoracic aorta extending down to the abdominal aorta. Aneurysm in the ascending aorta is the most common disease of thoracic aortic aneurysm in the aortic system. Thus one of the main reasons to investigate the flow phenomena in the aortic system is to understand its hemodynamic dependence on flow structure. The clinical impacts of understanding and formulating the effects of aortic geometry on vortex formation and the development of atherosclerosis justify the thorough unfolding of its structure.

A considerable number of experimental and numerical research works[1~8] have been conducted to study the flow dynamics and stresses in aortic system. Although a large number of investigations have led to better understanding of the flow disturbances induced by thoracic aortic aneurysm in the aortic system, most of the theoretical and experimental studies have been performed under different simplifying assumptions. It is well known that the regions near aortic curvature, branching, and bifurcation are predisposed to develop the atherosclerotic lesions[1,7]. The study of aorta, however, has been limited mainly due to human's lack of understanding of its complex network.

In this study, CT images of a healthy human aorta are used to extract the CFD aortic geometry and analyze the corresponding computational results. The human aortic arch model simulated in this study is generated using a set of CT images of a healthy female patient. The aim of this study was to evaluate the flow phenomena in the aortic model. Thus, we investigate the hemodynamic factors, such as secondary flow, wall pressure and wall shear stresses (WSS) in the model using commercial software ANSYS v18.1 tool[9].

MATHEMATICAL FORMULATION OF THE PROBLEM

A. The Geometric Model Construction

Starting from the medical images, the suitable geometry models were generated in order to conduct the desired blood flow simulations. Images produced from CTA are volume data with consisting of 210 aortic slices of 2172x1860 pixel images. MIMICS software imported these DICOM (Digital Imaging and Communications in Medicine) image files to reconstruct human aortic arch models. During segmentation the user creates 3D model based on the gray values within these DICOM files using thresholding. The user can apply the "region growing" tool to remove any floating pixels in the images and to separate the bone from the blood vessel. Finally the geometry models from the medical images coming from CTA shown in Figure 1 were obtained using the image segmentation and three-dimensional model creation using ANSYS Design Modeler software (Figure 1).

(a) Geometric model (b) Generated mesh

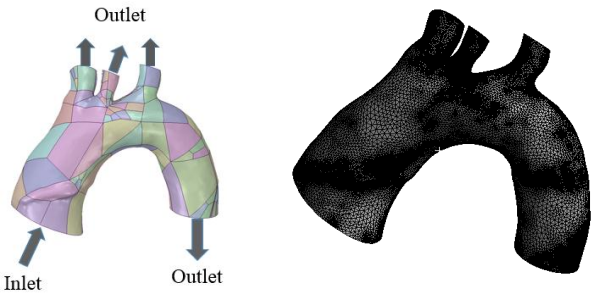

Figure 1: Extracted geometry from a set of CT images and the mesh model generated from Design Modeler

B. Governing Equations and Boundary Conditions

Numerical simulations were performed by using the commercial CFD software Fluent to determine the flow characteristics of the three-dimensional, pulsatile, incompressible and Newtonian fluid in aortic model. Although blood has a Non-Newtonian behavior, blood is considered a Newtonian fluid because the shear rates in large arteries are generally observed to be greater than 100 s^{-1}. Thus, the mass and momentum conservation equations for an incompressible Newtonian fluid neglecting the influence of body force, such as gravity, can be written as:

$$\nabla \bullet \vec{u} = 0 \tag{1}$$

$$\frac{\partial \vec{u}}{\partial t} + (\vec{u} \bullet \nabla)\vec{u} = -\frac{1}{\rho}\nabla \vec{P} + \frac{\mu}{\rho}\nabla^2 \vec{u} \tag{2}$$

where $\vec{u}$, ρ, and μ denote blood velocity vector, blood density (1,050kg/m^3), and blood dynamic viscosity (0.0035 Pa-s), respectively. α, the Womersley number, is defined as,

$$\alpha = \frac{D}{2}\sqrt{\frac{\rho\omega}{\mu}} \tag{3}$$

where D is the diameter of the aorta, μ is the blood viscosity, ω is the angular frequency of the oscillation.

For the simulation, the time-dependent physiological and uniform boundary condition shown in Figure 2[1)] was imposed at the inlet region[1)]. The aortic wall was assumed to be rigid, and no-slip condition was applied. The pressure boundary condition was applied to the outlets through the descending aorta and three major branches. In this simulation, the Womersley number, α, was approximately 18.8.

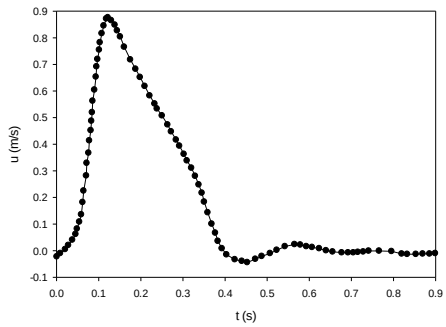

Figure 2: Inlet velocity wave form at inlet region

The governing equations were solved using the commercial software package FLUENT, ANSYS 18.1 (ANSYS Inc., Canonsburg, PA). The QUICK scheme was used to discretize the velocity and pressure variables using the PISO (Pressure Implicit with Splitting of Operators) algorithm. The implicit time-marching first-order scheme with the time step Δt=0.01 was used for the calculations, and the maximum iterations per time step was set to 5,000. To obtain the stable solutions, the computation performed four cardiac cycles and the result at the fourth cardiac cycle was used for the analysis in order to decrease numerical errors compared to the result at the third cardiac cycle less than 1%. The convergence tolerance for the continuity and velocity residuals was set at $5x10^{-5}$. Under those conditions, all solutions presented have been verified to be mesh-independent. Increasing the mesh density yields velocities that are within 1% of those shown here and flow separation zone lengths that are within 5% of those given. All simulations were performed using 2.9GHz Intel Xeon ® CPU E5-2667 (64GB of RAM) personal computer running Windows 7.

RESULTS AND DISCUSSION

A. Blood Flow Characteristics

Figure 3 shows the axial velocity profiles for the aortic arch model at the 6 selected time steps. The inflow at the inlet region accelerates early in the inlet velocity temporal waveform, and reaches a maximum of 0.87 m/sec at 0.12s. After this point, the velocity magnitude begins to decrease and drops to -0.044 m/sec at 0.45s (Figure 2). During the accelerating periods (Figure 3(a) and (b)) the flow is not reversed and the strong momentum prevents the flow from recirculation. Therefore streamlined flow stays forward with no recirculation. However in Figure 3(c) a flow disturbance begins near the inner wall of the arch due to the decelerating flow. In Figure 3(d), (e) and (f) a flow is complex and severely disturbed in the whole areas. This is mainly because of the secondary blood flow induced by the reverse flow in the ascending and descending aorta. When there is almost no flow in the axial direction, a strong secondary flow is seen both in the ascending and descending aorta as shown in Figure 3(d), (e) and (f).

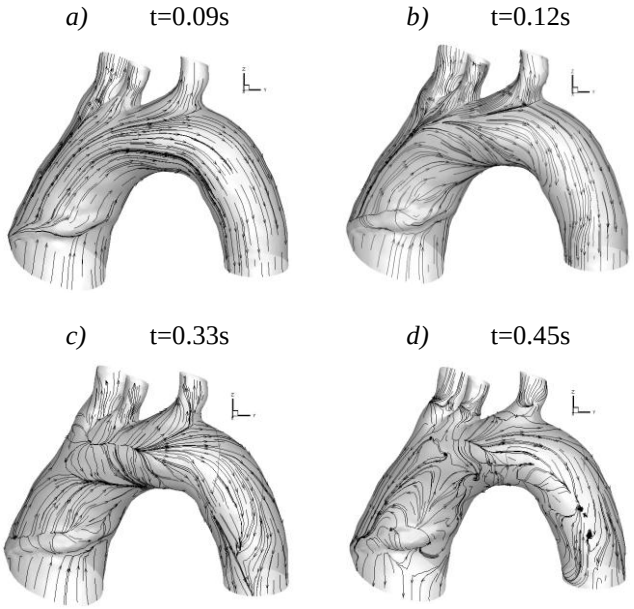

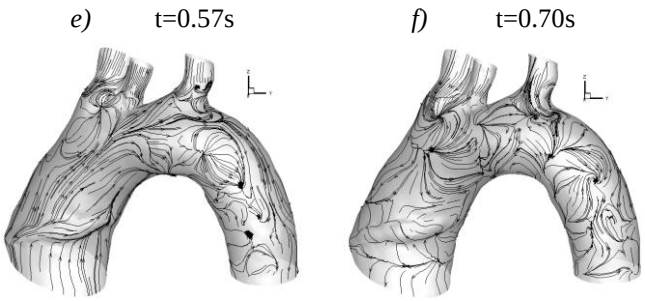

Figure 3: Axial velocity profiles at the six selected time steps

Figure 4 shows the velocity contour at the cross-sectional area at the aortic arch around the left subclavian artery as shown in Figure 4(e). During the systolic phase (Figure 4(a) and (b)) the velocity profiles were skewed toward the inner wall of the curvature in the cross-sectional area. During the diastolic phase, the blood flow reversed from the descending aorta to the ascending aorta in the inner wall region. As seen Figure 4(c) and (d) the flow is recirculated from the outer wall to the inner wall region.

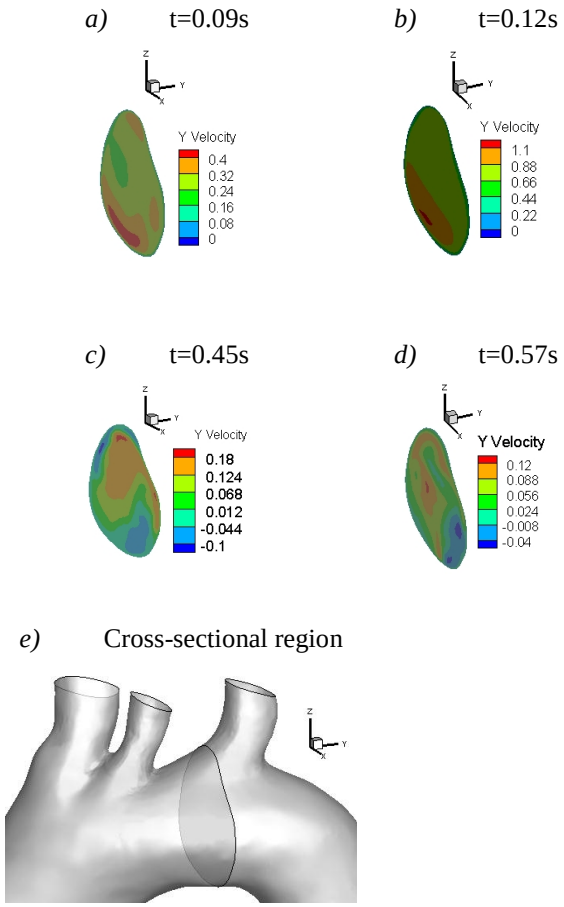

Figure 4: Velocity contours at the cross-sectional area at the aortic arch around the left subclavian artery

B. Wall Shear Stress and Pressure Distributions

A higher and lower WSS were considered to cause the intimal dysfunction as the development of the atherosclerotic lesion. For instance, the severely curved and bifurcated arteries such as aortic arch can cause the complex blood flow patterns to develop the atherosclerotic lesion.

Figure 5 shows the wall shear stress (WSS) distributions along the aortic arch wall. The results showed that a high WSS region occurred around branches at the top of the aortic arch. The maximum WSS occurs at the branches during the accelerating and peak systolic period. It is noted that there was a region of severely higher WSS at the distal sites of each branch and at the initial region of ascending aorta in accelerating phase. As blood flow increases, the wall shear stress is greatly increased in the whole aorta region. During the decelerating phase of systole, the low wall shear stress occurred at the outer wall in the ascending aorta as well as the left subclavian artery region. During the diastolic phases, the low WSS existed homogenously in the whole geometry.

The magnitudes of WSS decrease with decreasing blood velocity. The magnitudes of WSS under a low velocity blood flow, for instance at t=0.45 and 0.70, are much smaller than at a high velocity flow at t=0.09 and 0.12.

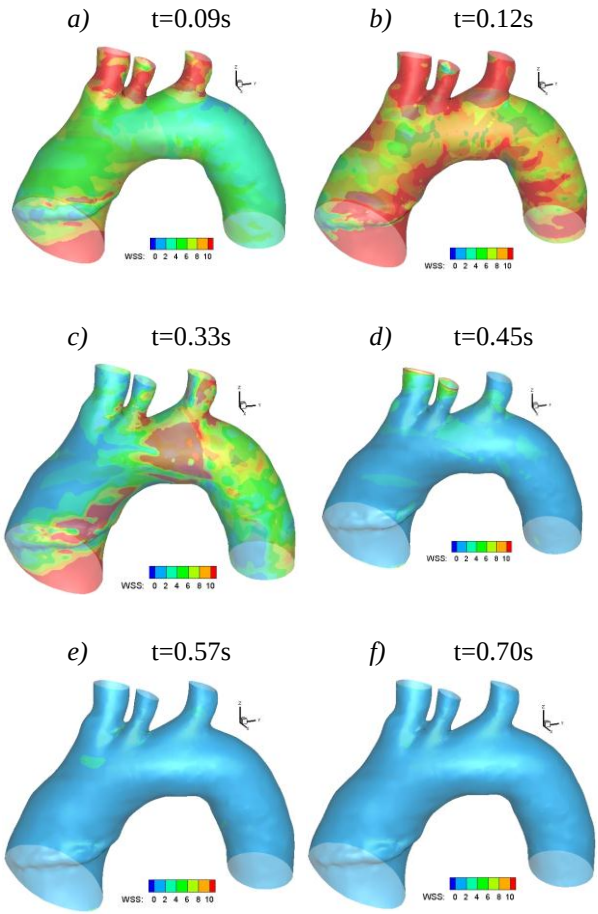

Figure 5: Wall shear stress distributions at the six selected time steps

Figure 6 shows the wall pressure distributions along the aortic arch wall. When the blood flow is accelerated with a strong momentum as shown in Figure 6(a), the pressure distribution in the model geometry is uniformly distributed in the blood flow direction. It is found that the pressure in the model is larger in the descending aorta when the back stream flows as shown in Figure 6(b) and (d). However, if the blood flow has locally maximum value during the diastolic period (see Figure 6(c)), the pressure distribution is reversed and favorable distribution in the flow direction.

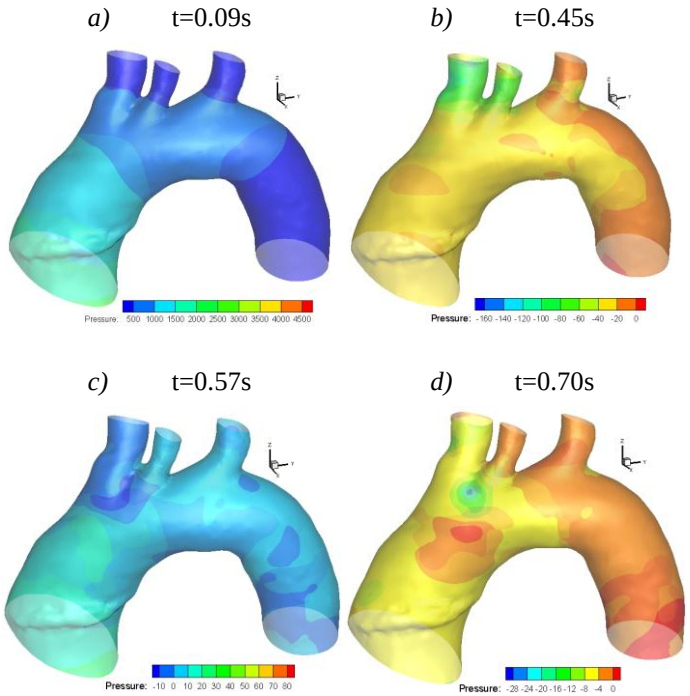

Figure 6: Wall pressure distributions at the four selected time steps

CONCLUDING REMARKS

In this study, we investigated the hemodynamic parameters of the human aortic arch geometry during the cardiac cycle. The CFD simulation is conducted to understand the flow characteristics under the assumption of rigid aorta wall and Newtonian fluid. The results of the simulations have revealed the following;

1) When there is almost no flow in the axial direction, a strong secondary flow is seen both in the ascending and descending aorta.

2) During the decelerating phase of systole, the low wall shear stress occurred at the outer wall in the ascending aorta as well as the left subclavian artery region.

3) During the diastolic phase, the blood flow reversed from the descending aorta to the ascending aorta in the inner wall region.

4) The pressure in the model is larger in the descending aorta when the back stream flows.

ACKNOWLEDGMENT

This work was supported by the National Research Foundation of Korea (NRF) grant funded by the Ministry of Education (Grant No. 2017R1D1A1B03028828)."

REFERENCES

[1] S. Jin, J. Oshinski, and D.P. Giddens “Effects of Wall Motion and Compliance on Flow Patterns in the Ascending Aorta,”, J. Biomech. Engng., Vol. 125, pp.347–354, June 2003.

[2] J.R. Nanduri, F.A. Pino-Romainville, and I. Celik, “CFD Mesh Generation for Biological Flows: Geometry reconstruction using Diagnostic Images,” Computers & Fluids, vol. 38, pp. 1026-1032, 2009.

[3] P. Ruengsakulrach, A.K. Joshi, S. Fremes, J. Butany, S. Foster, B. Wiwatanapataphee and Y. Lenbury, “Wall Shear Stress and Atherosclerosis: Numerical Blood Flow Simulations in the Mouse Aortic Arch,” 12th WSEAS Int. Conf. on Applied Mathematics, pp. 199–207, Dec. 2007.

[4] A.C. Benim, A. Nahavandi, A. Assmann, D. Schubert, P. Feindt and S.H. Suh, “Simulation of Blood Flow in Human Aorta with Emphasis on Outlet Boundary Conditions,” Applied Math. Modelling, Vol. 35, pp. 3175-3188, 2011.

[5] Y. Tokuda, M.H. Song, Y. Ueda, A. Usui, T. Akita, S. Yoneyama and S. Maruyama, “Three-Dimensional Numerical Simulation of Blood Flow in the Aortic Arch during Cardiopulmonary Bypass,” Euro. J. Cardio-Thor. Surg., Vol. 33, pp.164-167, 2008.

[6] C.Y. Wen, A.S. Yang, L.Y. Tseng and J.W. Chai, “Investigation of Pulsatile Flowfield in Healthy Thoracic Aorta Models,” Annals Biomed. Engng., Vol. 38 (2), pp.391-402, 2010.

[7] S. Numata, K. Itatani, K. Kanda, K. Doi, S. Yamazaki, K. Morimoto, K. Manabe, K. Ikemoto and H. Yaku, “Blood Flow Analysis of the Aortic Arch using Computational Fluid Dynamics,” Euro. J. Cardio-Thor. Surg., Jan. 20, pp.1-8, 2016.

[8] D. Mori, T. Havasaka and T. Yamaguchi, “Modeling of the human aortic arch with its major branches for CFD simulation of the blood flow,” JSME International J., Series C, Vol. 45, pp.997-1002, 2002.

[9] ANSYS Manuals version 18.1